BIOCHEMISTRY
including biophysical chemistry & molecular biology

ARTICLE

pubs.acs.org/biochemistry

Crystal Structures of *Parasponia* and *Trema* Hemoglobins: Differential Heme Coordination Is Linked to Quaternary Structure

Smita Kakar,[†] Ryan Sturms,[†] Andrea Tiffany,[†] Jay C. Nix,[‡] Alan A. DiSpirito,[†] and Mark S. Hargrove*[,†]

[†]Department of Biochemistry, Biophysics, and Molecular Biology, Iowa State University, Ames, Iowa 50011, United States

[‡]Advanced Light Source, Lawrence Berkeley National Laboratory, Berkeley, California 94720, United States

ABSTRACT: Hemoglobins from the plants *Parasponia andersonii* (ParaHb) and *Trema tomentosa* (TremaHb) are 93% identical in primary structure but differ in oxygen binding constants in accordance with their distinct physiological functions. Additionally, these proteins are dimeric, and ParaHb exhibits the unusual property of having different heme redox potentials for each subunit. To investigate how these hemoglobins could differ in function despite their shared sequence identity and to determine the cause of subunit heterogeneity in ParaHb, we have measured their crystal structures in the ferric oxidation state. Furthermore, we have made a monomeric ParaHb mutant protein (I43N) and measured its ferrous/ferric heme redox potential to test the hypothesized link between quaternary structure and heme heterogeneity in wild-type ParaHb. Our results demonstrate that TremaHb is a symmetric dimeric hemoglobin similar to other class 1 nonsymbiotic plant hemoglobins but that ParaHb has structurally distinct heme coordination in each of its two subunits that is absent in the monomeric I43N mutant protein. A mechanism for achieving structural heterogeneity in ParaHb in which the Ile$^{101(F4)}$ side chain contacts the proximal His$^{105(F8)}$ in one subunit but not the other is proposed. These results are discussed in the context of the evolution of plant oxygen transport hemoglobins, and other potential functions of plant hemoglobins.

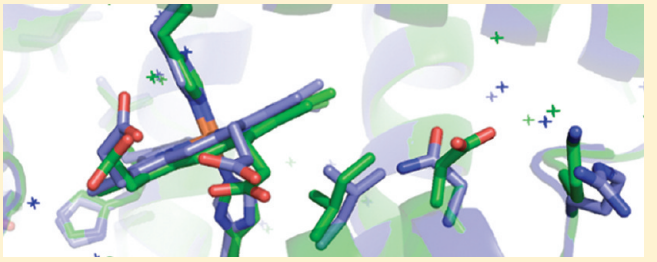

Plants and animals contain different classes of hemoglobins (Hbs) with distinct structures and functions.[1,2] Animals have oxygen transport Hbs along with others whose functions are not completely clear.[3] In plants, the class 1 nonsymbiotic Hbs (nsHbs) are believed to scavenge nitric oxide during nitrate assimilation under hypoxic conditions,[4,5] while the leghemoglobins are transporters and scavengers of oxygen inside the root nodules of legumes capable of symbiotic nitrogen fixation.[6] Oxygen transport is not the original function of Hbs in plants or animals,[3,7] and understanding the structural changes that accompanied its development will reveal clues about molecular evolution and protein design in the globin scaffold.

Oxygen transport Hbs evolved in animals nearly 500 million years ago, and the resulting proteins, myoglobin and the subunits of red blood cell hemoglobin, are <20% identical in sequence to their nontransport counterparts, including neuroglobin and cytoglobin.[8−10] In plants, oxygen transport Hbs evolved twice.[2,11−14] The first time, around 200 million years ago, resulted in the production of the leghemoglobins from class 2 nsHbs, which are ∼40% identical in sequence. The second event, originating from class 1 nsHbs, produced the oxygen transport Hb found in the root nodules of *Parasponia andersonii*, a non-legume capable of symbiotic nitrogen fixation. This more recent occurrence has left pairs of proteins with very high (>90%) levels of sequence identity, but clearly distinct physiological function.[12]

A comparison of *Parasponia* Hb (ParaHb) to that from *Trema tomentosa* (TremaHb), a class 1 nsHb 93% identical in sequence, showed that these two proteins have distinct oxygen affinities and kinetics that are characteristic of their physiological functions.[15] Furthermore, both Hbs are tightly dimeric in quaternary structure compared to other class 1 nsHbs,[16] and ParaHb is unusual in displaying two Fe^{3+}/Fe^{2+} redox potentials, presumably resulting from different values for each subunit. In contrast, most other Hbs, including TremaHb and the $\alpha_2\beta_2$ heterotetramer found in mammalian red bloods cells, exhibit a single redox midpoint indicative of thermodynamic exchange between the subunits.[15,17]

To investigate the proposed linkage of quaternary structure and heme chemistry in ParaHb and to provide a clearer structural framework for studying the evolutionary gain of oxygen transport function, we have used X-ray crystallography to examine the structures of ParaHb and TremaHb. We have also used site-directed mutagenesis to produce a monomeric version of ParaHb and measured its midpoint reduction potential in comparison to that of wild-type ParaHb. Our results reveal that the ParaHb subunits are indeed structurally distinct and that the biphasic redox potential is linked to quaternary structure and not observed in monomeric ParaHb.

MATERIALS AND METHODS

Protein Preparation. Codon-optimized cDNAs for *P. andersonii* (GenBank entry u27194) and *T. tomentosa* Hbs

Received: February 16, 2011
Revised: April 11, 2011
Published: April 14, 2011

Table 1. Data Collection and Refinement Statistics

	native TremaHb	SAD TremaHb	ParaHb
	Data Collection		
wavelength (nm)	1.54	1.72	1.54
resolution (Å)	31.3−1.84 (1.9−1.84)[a]	50−2.01 (2.08−2.01)[a]	39.19−2.15 (2.21 to 2.15)[a]
R_{merge} (%)	0.064 (0.297)[a]	0.056 (0.273)[a]	0.043 (0.307)[a]
completeness (%)	75.7 (14.9)[a]	87.8 (52.4)[a]	95.0 (90.0)[a]
no. of reflections (unique, total)	23821, 150655	89616, 619984	18471, 109909
redundancy	6.31 (2.10)[a]	7.0 (3.80)[a]	5.94 (5.05)[a]
	Refinement/Quality Statistics		
space group	*P*212121		*P*212121
unit cell dimensions			
bond lengths (Å)	a = 55.87, b = 70.74, c = 89.59		a = 55.04, b = 72.04, c = 88.32
bond angles (deg)	α = 90, β = 90, γ = 90		α = 90, β = 90, γ = 90
no. of molecules in the asymmetric unit	2		2
no. of refined residues, waters	310, 250		310, 148
R_{cryst} (%) (no NCS restraints)	21.31		22.44
R_{cryst} (%) (NCS restraints)	22.09		25.06
R_{free} (%)[b](no NCS restraints)	24.85		28.56
R_{free} (%) (NCS restraints)	26.07		32.50
average *B* factor (Å^2)	27.2		41.58
Ramachandran plot			
most favored (%)	99.0		98.9
additionally allowed (%)	1.0		1.1
generously allowed (%)	0		0
root-mean-square deviation			
bond lengths (Å)	0.008		0.013
bond angles (deg)	1.10		1.468

[a] Outer shell statistics are given in parentheses. [b] Calculated using 5% of the reflections.

(GenBank entry 1402313a) were synthesized and cloned as described previously.[15] The cDNA for ParaHb I43N was constructed using the Quickchange mutagenesis system from Agilent Technologies. TremaHb was expressed, and purification was achieved using a three-step process as described previously.[15] ParaHb and I43N ParaHb were expressed in host strain BL21 Star DE3 cells. Purification included ammonium sulfate fractionation, DEAE-cellulose, and CM-Sephadex column chromatography. The purification efficiency for the proteins used for crystallization was measured by the ratio of absorbance at the Soret peak and that at 280 nm and was 3.2 and 2.9 for TremaHb and ParaHb, respectively. The proteins were oxidized by addition of a slight molar excess of potassium ferricyanide that was removed by passage through a G-25 size exclusion column equilibrated with 10 mM HEPES buffer (pH 7.0). Ferrous hemoglobins were generated by reducing ferric samples with sodium dithionite. Absorbance spectra were recorded using a Cary-50 Bio spectrophotometer.

Crystallization and Data Collection. Crystals were grown using the hanging drop vapor diffusion method at 25 °C. Single crystals of TremaHb grew after 3 days from drops containing 1 μL of 3 mM ferric protein and 1 μL of crystallization buffer composed of 1.6 M ammonium sulfate and 0.1 M Hepes buffer (pH 7.0). ParaHb crystals grew overnight from drops containing 1 μL of 3 mM ferric protein and 1 μL of well buffer containing 1.6 M ammonium sulfate, 10% dioxane, and 0.1 M MES (pH 7.0) with 0.1 M phenol as an additive. Native diffraction data sets for TremaHb and ParaHb crystals were collected at 100 K on a Rigaku/MSC home source generator in the Iowa State University Macromolecular X-ray Crystallography Facility. Phasing of the TremaHb data set was accomplished using single-wavelength anomalous dispersion (SAD) at the iron atom, collected at the Advanced Light Source (beamline 4.2.2).

Structure Determination and Refinement. Diffraction data were integrated and processed using d*TREK.[18] Atomic positions for two iron atoms in the asymmetric unit of the TremaHb SAD data set were located by HKL2MAP (SHELXD),[19] and the phases were calculated with SOLVE.[20] Automated model building was performed using RESOLVE,[21] and manual model rebuilding with O[22] and PDB Viewer,[23] followed by refinement with REFMAC5 from the CCP4 suite.[24] The resolution of the TremaHb structure was extended to 1.84 Å using a native data set and further refinement using REFMAC5. The ParaHb structure was determined by molecular replacement starting with the TremaHb dimeric asymmetric unit. The final ParaHb structure resulted from refinement in CCP4. The final models have been deposited in the Protein Data Bank as entries 3QQR (ParaHb) and 3QQQ (TremaHb).

Quaternary Structure and Electrochemical Analysis of ParaHb I43N. The oligomeric state of the ferric ParaHb I43N mutant protein was determined by equilibrium analytical ultracentrifugation using the procedure published for wild-type ParaHb and TremaHb.[15] The molecular mass was calculated from the linear portions of the plots in Figure 4A

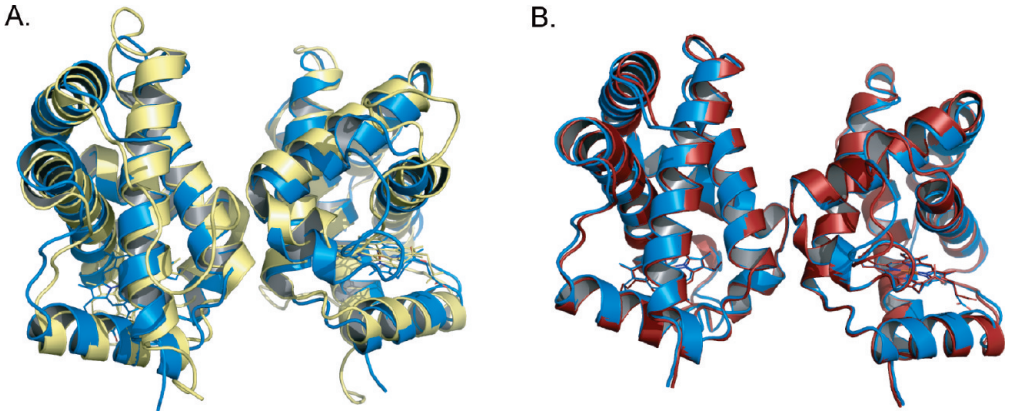

Figure 1. Crystal structures of *Parasponia* and *Trema* hemoglobins. Overlays of the structures of (A) ParaHb and TremaHb and (B) ParaHb and RiceHb1.

using eq 1

$$\ln(\text{Abs}) = \frac{M(1-\nu\rho)\omega^2}{2RT} r^2 \qquad (1)$$

where M is the molecular mass, r is the radial position of the sample, ν is the partial specific volume (fixed at 0.72 mL/g), ρ is the solvent density (fixed at 0.9982 g/mL), the angular velocity ω = 3099 rad/s (29600 rpm), $R = 8.31441 \times 10^7$ g cm^2 s^{-2} K^{-1} mol^{-1}, and T is 293 K.

Midpoint reduction potentials were measured using an apparatus described previously,[25] but with the following modifications. Rather than relying on nitrogen positive pressure to exclude oxygen, the titration apparatus was completely housed in an argon-purged inert box (Coy Laboratory Products). The anaerobic conditions were maintained using a palladium catalyst and a 5% hydrogen/argon gas mix. Midpoint potentials were obtained by fitting absorbance data to the following equation:

$$F_{\text{reduced}} = \frac{e^{-\left[\frac{nF(E_{\text{obs}} - E_{\text{mid}})}{RT}\right]}}{1 + e^{-\left[\frac{nF(E_{\text{obs}} - E_{\text{mid}})}{RT}\right]}} \qquad (2)$$

For wild-type ParaHb, which has two distinct redox transitions, the value was fit to a sum of two midpoint potentials with the amplitude of each fixed at 50%. However, allowing the amplitudes of each transition to float during the fitting routine yields the same results.

RESULTS

Structures of Ferric TremaHb and ParaHb. Crystals of ferric TremaHb and ParaHb diffracted to 1.8 and 2.15 Å, respectively. Neither home-source data set could be phased by molecular replacement using other nsHb structures as starting models, so phases were calculated experimentally for TremaHb, leading to a starting molecule for the refinement of the TremaHb structure, which in turn was a successful molecular replacement starting model for ParaHb. The best TremaHb model has two molecules in the asymmetric unit that can be refined using noncrystallographic symmetry (NCS) restraints.[26] The ParaHb model, however, was significantly improved by removing NCS restraints and allowing the subunits to adopt distinct structures (Table 1).

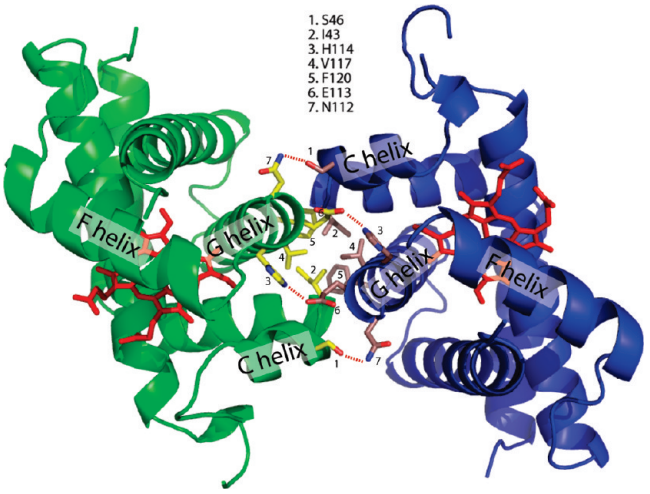

Figure 2. Detailed view of the dimer interface in ParaHb and TremaHb. The amino acid side chains constituting the interface of ParaHb and TremaHb include a hydrophobic cluster consisting of I43, V117, and F120 of each subunit that is conserved in other nsHbs, H-bonds between S49 and N112 of each subunit, and H-bonds between H114 and E113 of each subunit that are unique to these structures.

Quaternary Structure and Subunit Interface. The general organization of subunits in the dimeric structures of ParaHb and TremaHb resembles that of the asymmetric unit of rice nsHb (Figure 1),[27] having a symmetric group of hydrophobic contacts between the middle of the G helix of one subunit and the C helix of the other and a hydrogen bond between the side chain of a Ser on the C helix of one subunit and a polar side chain on the G helix of the other (Figure 2). The total buried surface area in the TremaHb and ParaHb dimers is ~600 Å^2 per subunit, slightly larger than that of rice nsHb1 (554 Å^2)[27] but still low compared to values for other stable dimers.[28] The increased stability of the TremaHb and ParaHb dimer (K_D < 1 μM) compared to those of other nsHbs (K_D ~ 80 μM) can be attributed to an additional symmetric pair of tight (2.7 Å) hydrogen bonds directly between the G helices of each subunit, created by the side chains of Glu^{113} and His^{114}. Another contributing factor could be that Ser^{46} forms hydrogen bonds with Asn^{112} in TremaHb and ParaHb, which is one turn of the G helix toward the N-terminus of the protein compared to the Glu side chain contacting this Ser side chain in other nsHbs.[16]

dx.doi.org/10.1021/bi2002423 |*Biochemistry* 2011, 50, 4273–4280

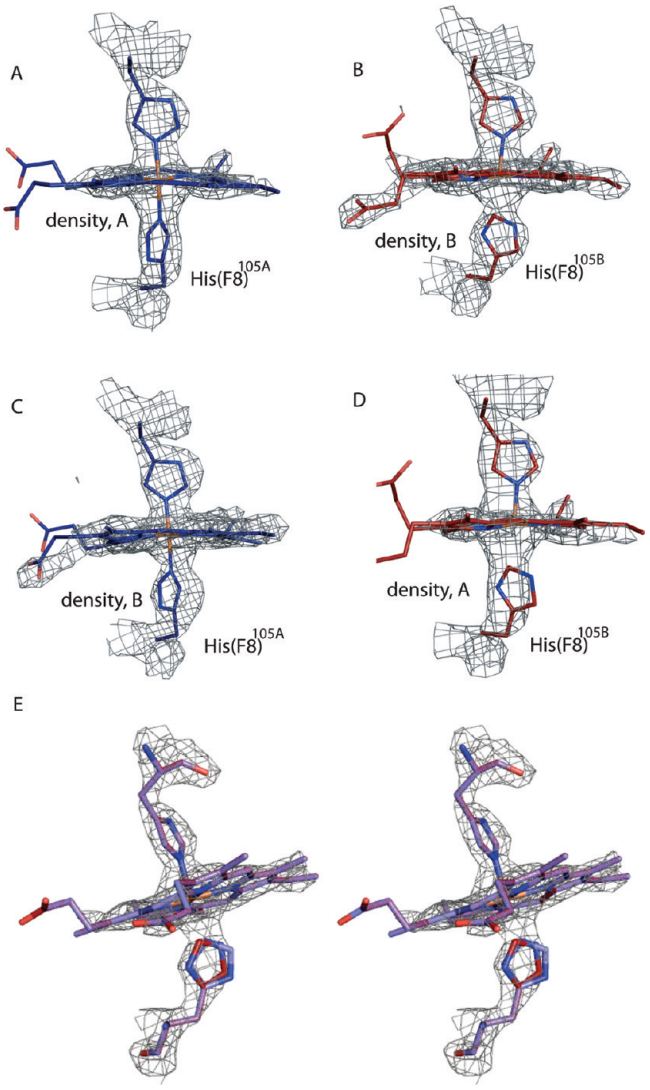

Figure 3. Heme pocket electron density of ParaHb subunits justifying distinct proximal histidine conformations. (A) Chain A model with chain A density. (B) Chain B model with chain B density. (C) Chain A model with chain B density. (D) Chain B model with chain A density. (E) Stereoview comparison of two possible χ_2 rotamers of the chain B His$^{105(F8)}$ side chain fit into the chain B electron density. The orientation used in panels A−D is colored red; the other, with Nε coordinating the heme iron, is colored blue. All electron density maps are contoured at 2.5σ.

ParaHb Has Structurally Distinct Subunits. While the TremaHb model did not improve much with the removal of NCS constraints [only 1.2% increase in R_{free} (Table 1)], that of ParaHb improved nearly 4% in both. A comparison of electron density in the two subunits of ParaHb reveals the most notable difference at the proximal histidines [His$^{105(F8)}$] (Figure 3). The ParaHb chain A proximal His is typical of Hbs (and similar to the subunits of TremaHb), with proper coordination geometry and a Nε−heme iron distance of 1.99 Å, but that of chain B is unusual. The electron density defining chain B His$^{105(F8)}$ clearly indicates the position of the main chain atoms and the side chain Cβ, but rotation of the side chain about χ_2 (the rotational orientation of the imidazole ring) is not as well defined.

Our efforts to resolve the position of the chain B His$^{105(F8)}$ side chain are presented in Figure 3. On the basis of the electron density, there are two χ_2 rotamers of the chain B His$^{105(F8)}$ side chain that must be considered. The best fit to the density results from rotating the chain A His$^{105(F8)}$ side chain by 117°, but this places Nε into a position from which it cannot coordinate the heme iron. To illustrate the necessity of fitting His$^{105(F8)}$ differently in chains A and B of ParaHb, the electron density for the hemes and the distal and proximal histidines for each are shown in Figure 3. Figure 3A shows the chain A heme pocket (blue) fit into chain A electron density. Figure 3B shows the chain B model (red) and its accompanying electron density. In panels C and D of Figure 3, the models and densities are swapped, showing the resulting poor fits of each model in the other's electron density.

An alternative chain B His$^{105(F8)}$ conformation that allows Nε−heme coordination (at 2.1 Å) results from χ_2 rotation by 73° of the chain A His position, but it extends the Nδ and Cε atoms outside of the electron density (Figure 3E). In support of this conformation is continuous electron density (albeit weaker than that in chain A) between the chain B His$^{105(F8)}$ side chain and the heme iron. Thus, the density immediately around the side chain supports the former (noncoordinated) conformation, but that between the side chain and the heme iron supports the latter (coordinated). Including both rotamers in the model did not improve model statistics, and fitting for the occupancy of both returned 100% of the former (noncoordinated) conformation. However, the density in this area of chain B and the resolution of the structure (2.15 Å) leave the exact nature of the His$^{105(F8)}$−heme interaction somewhat ambiguous. A prudent interpretation of these results (in combination with the ParaHb solution spectral data) is that the chain B His$^{105(F8)}$ side chain is distinct from that in chain A and is partially disrupted in heme coordination.

ParaHb Heme Pocket Heterogeneity Is Linked to Quaternary Structure. To test whether the asymmetric hemes in the structure of ParaHb are the root of the biphasic reduction potentials observed for the wild-type protein, a point mutation (I43N) was introduced into the hydrophobic core of the dimer interface with the goal of producing a monomeric ParaHb protein. This particular substitution was chosen because a homologous mutation in rice nsHb was previously used to disrupt quaternary structure without otherwise affecting the protein.[16] To measure the effects of the I43N mutation on the quaternary structure of ParaHb, the molecular mass of the mutant protein was measured by equilibrium analytical ultracentrifugation (Figure 4A). The experiment was conducted with 5 μM (in heme) wild-type and I43N ParaHb, and molecular masses were calculated to be 31.1 and 14.3 kDa, respectively, indicating that the mutant protein is monomeric at this concentration.

The consequences of disrupting the ParaHb dimer were measured by comparing the ferric and ferrous absorption spectra of the wild-type and I43N proteins and by measuring the reduction potential of the heme iron using potentiometric titration while monitoring the absorption spectra. Panels B and C of Figure 4 show the absorbance spectra of wild-type and I43N ParaHb in the ferric and ferrous oxidation states, respectively. The ferric absorption spectra are similar, exhibiting the mixed-spin state associated with the shoulder at 625 nm and the lower absorbance at 540 nm compared to that of rice nsHb1, which is fully low-spin. However, the ferrous absorbance spectra of these proteins are different. Wild-type ParaHb is largely high-spin, with a slight (~15%) contribution of low-spin character. In contrast, the I43N mutant protein is completely high-spin, with no indication of hexacoordination by the distal His. In Figure 4, rice nsHb1 again serves as the control for hxHb with a low-spin spectrum.

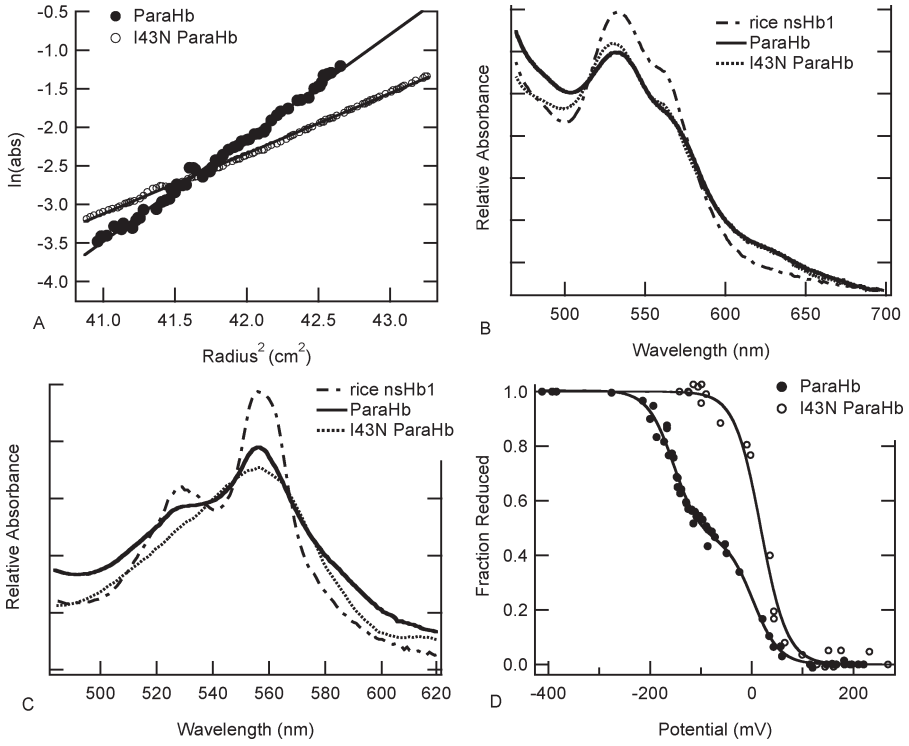

Figure 4. Physical analysis of wild-type and I43N ParaHb. (A) Each ferric Hb was analyzed by equilibrium analytical ultracentrifugation at 410 nm, at a concentration of 5 μM. The slopes of these plots yield molecular masses of 31.1 and 14.3 kDa for wild-type and I43N ParaHb, respectively. (B and C) Absorbance spectra of ferric (B) and ferrous (C) ParaHb and I43N ParaHb along with RiceHb1 as a control. (D) Potentiometric titrations of wild-type and I43N ParaHb. These curves were fit to eq 2 to extract midpoint redox potentials for each protein. For wild-type ParaHb, the curve fit to a sum of two midpoints at 0 and −150 mV (vs SHE), and for the I43N mutant protein, a single midpoint is observed at 17 mV.

The spectrochemical redox titrations for wild-type and I43N ParaHb are shown in Figure 4D. As previously described, wild-type ParaHb exhibits the unusual phenomenon of two discrete midpoint potentials at 0 and −150 mV.[15] However, the reduction of the monomeric ParaHb I43N mutant protein is monophasic with a midpoint reduction potential of 17 mV, which is different from either of the wild-type midpoint potentials, and supportive of a linkage between quaternary structure and heme heterogeneity.

DISCUSSION

The crystal structures of ParaHb and TremaHb reflect the relationship between their primary structures and in vitro biochemistry; these are two proteins sharing many general similarities along with a few key differences that are critical to their distinct physiological functions. Similarities include tight dimeric quaternary structure and relatively weak bis-histidyl coordination in the ferrous oxidation state. Functional differences include a lower oxygen affinity and a faster oxygen dissociation rate constant in ParaHb, consistent with its function as an oxygen transporter. TremaHb, on the other hand, exhibits oxygen binding constants on par with those of other class 1 nsHbs.[1,15] The structures of these proteins are very similar and do not offer an immediate explanation for the differences in their oxygen binding abilities.

A comparison of the ParaHb and TremaHb structures presents some other differences between the proteins that could be linked to oxygen binding, but the mechanism of linkage is not readily evident. The subunits of ferric ParaHb have distinct heme sites; one resembles a typical bis-histidyl Hb, and the other is largely pentacoordinate with the proximal histidine [His$^{105(F8)}$] dissociated from the heme iron. These observations bring to the forefront several questions related to plant Hb structure and function.

How Could the Structure of ParaHb Cause Asymmetric Heme Sites and Affect Oxygen Affinity? Absorbance spectra of ParaHb suggest that it is an equal mixture of pentacoordinate and hexacoordinate heme in the ferric oxidation state. The biphasic redox potentials and structural differences between the subunits support the hypothesis that the mixture of high- and low-spin hemes results from discrete and nonexchanging heme environments, rather than equivalent subunits at equilibrium between high- and low-spin states. There are no indications from kinetic measurements of oxygen or CO binding that the ferrous subunits behave differently, suggesting that heme site asymmetry may be relieved when the protein is reduced. However, the possibility of heterogeneous ligand binding to the distinct chains of ferric ParaHb (or even binding to the proximal side of the heme group in chain B) cannot yet be discounted.

It is clear that heme asymmetry is induced by the subunit interface, as the monomeric mutant protein I43N ParaHb does not exhibit biphasic redox titration. The absorbance spectrum of ferric I43N ParaHb is a mixture of high- and low-spin hemes, suggesting that the monomeric ParaHb heme pocket does not favor either state completely in the absence of influence by the subunit interface. However, when reduced, the I43N mutant protein is completely high-spin, indicating that the residual (~10%) low-spin character in wild-type ferrous ParaHb is induced by the dimer interface.

There are only 11 differences between the primary structures of ParaHb and TremaHb.[15] None of them are near the subunit

dx.doi.org/10.1021/bi2002423 |*Biochemistry* 2011, 50, 4273–4280

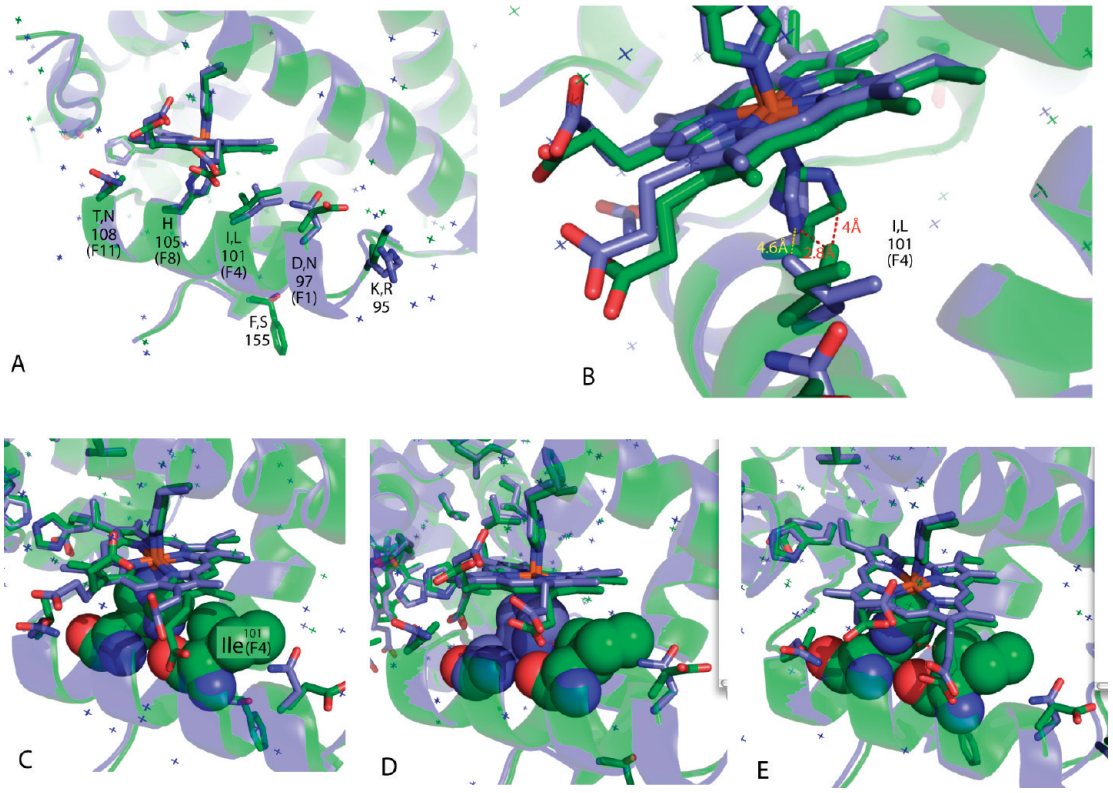

Figure 5. Potential role for ParaHb Ile^{101} in stimulating heme asymmetry. (A) Five of the 11 differences between ParaHb (green structure) and TremaHb (lavender structure) are on or near the F helix. Each is labeled with the ParaHb amino acid first and the TremaHb amino acid second (for example, I,L means that ParaHb has Ile at this position and TremaHb has a Leu). (B) ParaHb chain B compared to TremaHb. (C) Space-filling representation of ParaHb chain A showing an acceptable van der Waals contact between Ile$^{101(F4)}$ and His$^{105(F8)}$. (D) Space-filling representation of ParaHb chain B with His$^{105(F8)}$ from chain A, showing the steric clash that would result if His$^{105(F8)}$ of chain B adopted this orientation. (E) Space-filling representation of ParaHb chain B, showing the acceptable van der Waals contact between Ile$^{101(F4)}$ and His$^{105(F8)}$ observed when the His$^{105(F8)}$ side chain is displaced from the heme iron.

interface, and six are remote from the heme and present no obvious mechanism for influencing heme chemistry. The other five are located on (or near) the F helix around the proximal His$^{105(F8)}$ and are the most likely to affect coordination to the heme iron (Figure 5). Of these, the amino acid at sequence position 101(F4) in each protein contacts His$^{105(F8)}$ and provides a plausible mechanism for displacing the ParaHb chain B His$^{105(F8)}$ side chain from the heme iron.

The His$^{105(F8)}$ side chain of TremaHb is coordinated to the heme iron in both subunits, and steric contact between the Leu$^{101(F4)}$ and His$^{105(F8)}$ side chains is minimal, with the shortest distance (between Cδ and Nδ of each side chain) being 4.6 Å. The substitution of Ile at this position in ParaHb creates a much shorter distance between the His$^{105(F8)}$ side chain and the Cγ ("β-branched") Ile$^{101(F4)}$ methyl group. In ParaHb chain A, which has His$^{105(F8)}$ side coordination like TremaHb, there is a short (but acceptable) 3.44 Å contact between Ile$^{101(F4)}$ Cγ and His$^{105(F8)}$ Nδ. However, if the same orientation of His$^{105(F8)}$ were found in chain B, this distance would be 2.8 Å, causing a severe steric clash[29] (Figure 5B–D). Instead, His$^{105(F8)}$ is found at the observed position, creating an acceptable 4.0 Å contact between Ile$^{101(F4)}$ Cγ and His$^{105(F8)}$ Cδ (Figure 5E).

It is not completely clear how the differential interactions between Ile$^{101(F4)}$ and His$^{105(F8)}$ in ParaHb might be influenced by the subunit interface. However, there are some significant differences between the subunit interfaces in ParaHb and TremaHb in comparison to those of other nsHbs that are probably important.[1,27,30] In ParaHb and TremaHb, there are three successive side chains at the beginning of the G helix that are directly involved in the subunit interface: Asn^{112}, Glu^{113}, and His^{114} (Figure 2). The intersubunit contact between Glu^{113} and His^{114} is not present in any other nsHb structures to date and serves as a direct interaction between the G helices of the subunits. The contact between Asn^{112} and Ser^{46} is also different from those of other nsHbs, where the homologous Ser instead contacts a Glu side chain two turns farther down the G helix, away from the F helix.

Thus, ParaHb and TremaHb have unique subunit contacts at the beginning of the G helix that could influence the environment of the F helix and His$^{105(F8)}$. In the context of ParaHb, this unique subunit interface could work in concert with Ile$^{101(F4)}$ to stimulate the differences in coordination between the two subunits and potentially influence the observed differences in oxygen affinity between the two proteins. Detailed studies of site-directed mutations of ParaHb and TremaHb are required to investigate this hypothesis.

What Is the Role of Quaternary Structure in nsHb Function? Not all Hbs have quaternary structure, and it seems logical that those exhibiting it do so for a reason. Many, including red blood cell Hb, use subunit interactions to achieve cooperative oxygen binding. Others, such as many extracellular Hbs, probably do so for stability as well as cooperativity.[31,32] Quaternary

structure in Plant Hbs includes dimers ($K_{D,dimer}$ < 1 μM) in the cases of ParaHb and TremaHb, "loose" dimers ($K_{D,dimer}$ ~ 80 μM) in other nsHbs,[16,33] and monomeric leghemoglobins.[6] The quaternary structures of class 2 and class 3 nsHbs have not yet been measured.

Possible reasons for quaternary structure include cooperative ligand binding, stability, and electron transport events involving more than one electron, or electron transfer at different redox potentials. A role for quaternary structure in protein stability seems unlikely, as nsHbs and leghemoglobins are naturally stable in different quaternary states, and monomeric mutant proteins (like I43N ParaHb and others[16]) have not been challenging to make in the laboratory. There is no evidence of cooperative ligand binding in nsHbs, although equilibrium oxygen binding curves have not been measured directly. Until recently, it was believed that their high oxygen affinities precluded direct observation of equilibrium constants, but recent estimations of affinity for class 2 nsHbs and ParaHb suggest that these might be suited to this measurement.[1,15]

The involvement of quaternary structure in electron transfer reactions cannot be firmly evaluated without first knowing the biochemical function of nsHbs. This could be important in redox biochemistry involving nitrogen,[34] including nitric oxide scavenging,[35] by influencing heme reduction kinetics or redox chemistry with a substrate. Rather than being limited to a one-electron redox event such as nitric oxide dioxygenase-mediated nitric oxide scavenging,[36] dimeric nsHbs could also facilitate two-electron redox events. The distinct redox potentials of ParaHb subunits are intriguing, as this is not observed in other Hb systems. Normally, the hemes of multidomain Hbs are linked electronically, manifesting a single redox potential for the protein.[17]

How Do the Structures of ParaHb and TremaHb Impact Our Understanding of the Evolution of Plant Oxygen Transport Hbs? The fact that leghemoglobins and ParaHb differ in quaternary structure indicates that oxygen transport can be achieved in either quaternary structure and suggests that class 1 nsHbs (from which ParaHb is derived) and class 2 nsHbs (which gave rise to the leghemoglobins) followed different pathways in their independent evolution of this function. If we consider pre-oxygen transport Hbs to be similar to the class 1 and class 2 nsHbs, then there were different challenges to building an oxygen transporter from each.[1,15] The conversion of class 2 nsHbs to leghemoglobins required an increase in the oxygen affinity and an increase in the oxygen dissociation rate constant and settled on a monomeric protein. Conversion of a typical class 1 nsHb to ParaHb requires a lower oxygen affinity, a faster oxygen dissociation rate constant, and a tighter dimeric structure. Clearly, the formation of a tight dimer alone is not sufficient to make these changes, as TremaHb is also dimeric but retains the physical properties of class 1 nsHbs. The most likely explanation is that the tight dimer interface is involved in the mechanism of increasing the oxygen dissociation rate constant, causing a lower oxygen affinity in ParaHb. Thus, as in the comparison of myoglobin to leghemoglobin,[11] the physical requirements for oxygen transport can be implemented using different chemical mechanisms even in similar protein structures.

Accession Codes

Protein Data Bank entries 3QQQ and 3QQR.

AUTHOR INFORMATION

Corresponding Author

*Phone: (515) 294-2616. E-mail: msh@iastate.edu. Fax: (515) 294-0453.

ABBREVIATIONS

Hbs, hemoglobins; TremaHb, *T. tomentosa* hemoglobin; ParaHb, *P. andersonii* hemoglobin; nsHb, nonsymbiotic hemoglobin.

REFERENCES

(1) Smagghe, B., Hoy, J., Percifield, R., Kundu, S., Hargrove, M., Sarath, G., Hilbert, J., Watts, R., Dennis, E., Peacock, W., Dewilde, S., Moens, L., Blouin, G., Olson, J., and Appleby, C. (2009) Review: Correlations between oxygen affinity and sequence classifications of plant hemoglobins. *Biopolymers 91*, 1083–1096.

(2) Kakar, S., Hoffman, F. G., Storz, J. F., Fabian, M., and Hargrove, M. S. (2010) Structure and reactivity of hexacoordinate hemoglobins. *Biophys. Chem. 152*, 1–14.

(3) Hankeln, T., Ebner, B., Fuchs, C., Gerlach, F., Haberkamp, M., Laufs, T. L., Roesner, A., Schmidt, M., Weich, B., Wystub, S., Saaler-Reinhardt, S., Reuss, S., Bolognesi, M., De Sanctis, D., Marden, M. C., Kiger, L., Moens, L., Dewilde, S., Nevo, E., Avivi, A., Weber, R. E., Fago, A., and Burmester, T. (2005) Neuroglobin and cytoglobin in search of their role in the vertebrate globin family. *J. Inorg. Biochem. 99*, 110–119.

(4) Sowa, A., Duff, S., Guy, P., and Hill, R. (1998) Altering hemoglobin levels changes energy status in maize cells under hypoxia. *Proc. Natl. Acad. Sci. U.S.A. 95*, 10317–10321.

(5) Nie, X., and Hill, R. D. (1997) Mitochondrial Respiration and Hemoglobin Gene Expression in Barley Aleurone Tissue. *Plant Physiol. 114*, 835–840.

(6) Appleby, C. A. (1984) Leghemoglobin and Rhizobium Respiration. *Annu. Rev. Plant Physiol. 35*, 443–478.

(7) Wittenberg, B. (2001) Truncated Hemoglobins: A New Family of Hemoglobins Widely Distributed in Bacteria, Unicellular Eukaryotes, and Plants. *J. Biol. Chem. 277*, 871–874.

(8) Burmester, T., Welch, B., Reinhardt, S., and Hankeln, T. (2000) A vertebrate globin expressed in the brain. *Nature 407*, 520–523.

(9) Burmester, T., Ebner, B., Weich, B., and Hankeln, T. (2002) Cytoglobin: a novel globin type ubiquitously expressed in vertebrate tissues. *Mol. Biol. Evol. 19*, 416–421.

(10) Trent, J. T., III, and Hargrove, M. S. (2002) A ubiquitously expressed human hexacoordinate hemoglobin. *J. Biol. Chem. 277*, 19538–19545.

(11) Kundu, S., Trent, J. T., III, and Hargrove, M. (2003) Plants, humans and hemoglobins. *Trends Plant Sci. 8*, 387–393.

(12) Appleby, C. A., Tjepkema, J. D., and Trinick, M. J. (1983) Hemoglobin in a Nonleguminous Plant, *Parasponia*: Possible Genetic Origin and Function in Nitrogen Fixation. *Science 220*, 951–953.

(13) Guldner, E., Desmarais, E., Galtier, N., and Godelle, B. (2004) Molecular evolution of plant haemoglobin: Two haemoglobin genes in Nymphaeaceae *Euryale ferox*. *J. Evol. Biol. 17*, 48–54.

(14) Guldner, E., Godelle, B., and Galtier, N. (2004) Molecular adaptation in plant hemoglobin, a duplicated gene involved in plant-bacteria symbiosis. *J. Evol. Biol. 59*, 416–425.

(15) Sturms, R., Kakar, S., Trent, J. T., III, and Hargrove, M. S. (2010) Trema and parasponia hemoglobins reveal convergent evolution of oxygen transport in plants. *Biochemistry 49*, 4085–4093.

(16) Goodman, M. D., and Hargrove, M. S. (2001) Quaternary structure of rice nonsymbiotic hemoglobin. *J. Biol. Chem. 276*, 6834–6839.

(17) Eraldo Antonini, J. W., Brunori, M., Taylor, J. F., Rossi-Fanelli, A., and Caputo, A. (1964) Studies on the Oxidation-Reduction Potentials of Heme Proteins. *J. Biol. Chem. 239*, 907–912.

(18) Pflugrath, J. W. (1999) The finer things in X-ray diffraction data collection. *Acta Crystallogr. D55*, 1718–1725.

(19) Pape, T., and Schneider, T. R. (2004) HKL2MAP: A graphical user interface for macromolecular phasing with SHELX programs. *J. Appl. Crystallogr. 37*, 843–844.

(20) Terwilliger, T. C., and Berendzen, J. (1999) Automated MAD and MIR structure solution. *Acta Crystallogr. D55*, 849–861.

(21) Terwilliger, T. C. (2000) Maximum likelihood density modification. *Acta Crystallogr. D56*, 965–972.

(22) Jones, T. A., Zou, J. Y., Cowan, S. W., and Kjeldgaard, M. (1991) Improved methods for building protein models in electron density maps and the location of errors in these models. *Acta Crystallogr. D47* (Part 2), 110–119.

(23) Schwede, T., Kopp, J., Guex, N., and Peitsch, M. (2003) SWISS-MODEL: An automated protein homology-modeling server. *Nucleic Acids Res. 31*, 3381–3385.

(24) Collaborative Computational Project, Number 4. (1994) The CCP4 suite: Programs for protein crystallography. *Acta Crystallogr. D50*, 760–763.

(25) Halder, P., Trent, J. T., III, and Hargrove, M. (2007) Influence of the protein matrix on intramolecular histidine ligation in ferric and ferrous hexacoordinate hemoglobins. *Proteins 66*, 172–182.

(26) Adams, P. D., Grosse-Kunstleve, R. W., Hung, L.-W., Ioerger, T. R., McCoy, A. J., Moriarty, N. W., Read, R. J., Sacchettini, J. C., Sauter, N. K., and Terwilliger, T. C. (2002) PHENIX: Building new software for automated crystallographic structure determination. *Acta Crystallogr. D58*, 1948–1954.

(27) Hargrove, M. S., Brucker, E. A., Stec, B., Sarath, G., Arredondo-Peter, R., Klucas, R. V., Olson, J. S., and Phillips, G. N., Jr. (2000) Crystal structure of a nonsymbiotic plant hemoglobin. *Struct. Folding Des. 8*, 1005–1014.

(28) Janin, J., Miller, S., and Chothia, C. (1988) Surface, Subunit Interfaces and Interior of Oligomeric Proteins. *J. Mol. Biol. 204*, 155–164.

(29) Li, A. J., and Nussinov, R. (1998) A set of van der Waals and coulombic radii of protein atoms for molecular and solvent-accessible surface calculation, packing evaluation, and docking. *Proteins 32*, 111–127.

(30) Hoy, J., Robinson, H., Trent, J. T., III, Kakar, S., Smagghe, B., and Hargrove, M. (2007) Plant hemoglobins: A molecular fossil record for the evolution of oxygen transport. *J. Mol. Biol. 371*, 168–179.

(31) Zhu, H., Hargrove, M., Xie, Q., Nozaki, Y., Linse, K., Smith, S. S., Olson, J. S., and Riggs, A. F. (1996) Stoichiometry of subunits and heme content of hemoglobin from the earthworm *Lumbricus terrestris*. *J. Biol. Chem. 271*, 29999–30006.

(32) Royer, W. E., Jr., Hendrickson, W. A., and Chiancone, E. (1989) Structural transitions upon ligand binding in a cooperative dimeric hemoglobin. *Science 249*, 518–521.

(33) Duff, S. M., Wittenberg, J. B., and Hill, R. D. (1997) Expression, purification, and properties of recombinant barley (*Hordeum* sp.) hemoglobin. Optical spectra and reactions with gaseous ligands. *J. Biol. Chem. 272*, 16746–16752.

(34) Gupta, K. J., Fernie, A. R., Kaiser, W. M., and van Dongen, J. T. (2011) On the origins of nitric oxide. *Trends Plant Sci.16*, 160–168.

(35) Igamberdiev, A., and Hill, R. (2004) Nitrate, NO and haemoglobin in plant adaptation to hypoxia: An alternative to classic fermentation pathways. *J. Exp. Bot. 55*, 2473–2482.

(36) Eich, R. F., Li, T., Lemon, D. D., Doherty, D. H., Curry, S. R., Aitken, J. F., Mathews, A. J., Johnson, K. A., Smith, R. D., Phillips, G. N., Jr., and Olson, J. S. (1996) Mechanism of NO-induced oxidation of myoglobin and hemoglobin. *Biochemistry 35*, 6976–6983.